

Technische Universität München
Physik Department
Chair E12

Layer Thickness Measurement of organic Sectional Images

Bachelor Thesis of
Tobias Widmann

August 24, 2012

Erstgutachter (Themensteller):	Prof. W. Henning
Zweitgutachter:	Prof. P. Böni
Wissenschaftlicher Betreuer:	Dr. R. Gernhäuser

Summary

Mood disorder is a widespread illness in modern societies. Amongst others, lithium is administered for the treatment but the precise effect is still not investigated entirely. To examine whether the lithium eventually accumulates in the central nervous system, a new post mortem measurement method is being developed at the chair E12 of the Technische Universität München. The aim is to get a spatially resolved lithium concentration map of the human brain. However, the experiment currently under development yields the lithium concentration in units of $\mathrm{pg/cm^2}$. Hence, in order to obtain a medical relevant quantity in units of $\mathrm{pg/cm^3}$, the layer thickness of the examined brain tissue samples must be determined first. These thin slices of brain are supposed to have a thickness of $10\,\mu\mathrm{m}$, but during the fabrication process and by freeze drying them, several factors cause an inhomogeneous tissue thickness over the area of the samples. In this thesis, the thickness of the brain tissue is determined and additional measurements were performed to further investigate the properties of the samples.

In order to get the exact profile of the samples, they are bombarded with $5486\,\mathrm{keV}$ alpha particles from an $^{241}\mathrm{Am}$ source. Using a position sensitive Si-PIN-diode, the energy of the alpha particles after passing the tissue layer is measured. The average particle energy is determined and the energy loss is calculated by the use of a reference measurement. In order to obtain the tissue thickness the software SRIM is used to simulate the alpha particles' energy loss for different thicknesses14. Subsequently, the energy loss is converted to the layer thickness.

In this thesis, this has been performed for a series of 49 brain tissue samples. Furthermore, the freeze drying process and the foil to which the tissue gets attached was examined. Finally, in an attempt to improve the thickness measurement's accuracy, a way of experimentally determining the specific stopping power of alpha particles is tested. Therefore, the energy loss of tissue samples of a specified mass and area is measured. Using this calibration, the energy loss is converted into units of mass per area. Compared with the SRIM simulation, which does not consider several chemical properties of the samples, the tissue thickness deviates by 6 %.

The mean thickness of the brain tissue samples was measured to vary between $1{,}3\,\mu\mathrm{m}$ and $3{,}3\,\mu\mathrm{m}$. The spatial resolution of $\sigma_x = \sigma_y = 156\,\mu\mathrm{m}$ is nearly twice as high as that of the lithium experiment and the relative uncertainty in thickness amounts to 5% for a typical measurement. An additional uncertainty of $\Delta d = 20\,\mu\mathrm{m}$ is introduced by the inhomogeneity of the polyethylene foils on which the tissue samples are fixated.

By using the empty foil as a reference for the energy loss determination, this would be rectified and by improving the experimental setup, the measuring time could be greatly reduced in principle. Now, a practicable way of correctly combining the lithium areal density and the layer thickness needs to be found.

Table of Content

1. Motivation

Mood (affective) disorder is a mental disorder with its specific cause still being mostly unknown. Within the Diagnostic and Statistical Manual of Mental Disorders classification system, it is referred to a diagnose where a disturbance of the person's mood is the main aspect. It is mainly subdivided into two sorts of symptoms depending on whether there has been a manic or hypomanic phase in between the depressions or not. Mood disorder with such phases is called bipolar disorder (BD) whereas courses with solely depressive phases are assigned to the depressive disorders (DD). The depressive syndrome is characterized by an abnormal low mood, a reduced self-esteem, loss of interest and listlessness for normally enjoyable activities. Roughly 8,5% of the world's population have suffered at least once from it [1]. The course of the disorder can be long-lasting or episodic though the latter is more usual [2]. The maniac syndrome is distinguished by an extremely elevated or irritable mood and represents the opposite to the depression. A purely maniac course is rare and it is more common to alternate with phases of depression. It is estimated that approximately 9% of the world's population have suffered from different forms of bipolar disorder before [3]. The biological cause is suspected in a dysfunction of the communication of the neurotransmitters in the brain. Mood disorder should not be underestimated as at least 10% of the seriously depressive cases do conclude in suicide [2].

Lithium is administered as a mood-stabilizing drug and is therefore applied for the treatment and prophylaxis of mood disorders. Though many biochemical effects of lithium have been investigated, no final conclusion for the biological mechanism in the treatment of mood disorders can be made. After ingestion, it is widely spread throughout the central nervous system, interacting with neurotransmitters and receptors. During the next 12 hours 50% of the lithium gets egested and the other half is reduced over one or two weeks [4]. This delayed elimination is caused by an accumulation of lithium in the cells, which, in turn, is used to examine the distribution and concentration of lithium within samples of the central nervous system of deceased patients that ingested lithium for several weeks or longer. These measurement results are compared to samples of untreated patients to investigate at which parts of the brain lithium gets accumulated and takes effect.

2. Trace element detection of lithium in organic tissue with neutrons

There exist different methods to determine the amount of lithium in organic tissues, but the most commonly used are either lacking spatial resolution or suffer from high detection limits [5]. Therefore a new measuring process is being developed at the Physics Department at the chair E12 of the Technische Universität München by Josef Lichtinger.

2.1. Experimental method

For Josef Lichtinger's experiment, $10\mu m$ thin samples of brain tissue are attached to a specially fabricated holder. These samples are exposed to a neutron beam triggering the reaction $^6\mathrm{Li} + \mathrm{n} \rightarrow \alpha + \mathrm{T}$. $^6\mathrm{Li}$ has a capture cross section for thermal neutrons of $940\,\mathrm{barn}$ and this two particle decay dominates over all other decay channels [6]. Moreover, since the initial $^6\mathrm{Li}$ is static in the laboratory frame and there are only two particles of similar mass in the decay channel, these will be, due to momentum conservation, emitted into opposite directions with similar kinetic energy. For the experiment the samples are located in between a set of position sensitive detectors (PSD) as shown in Figure 1.

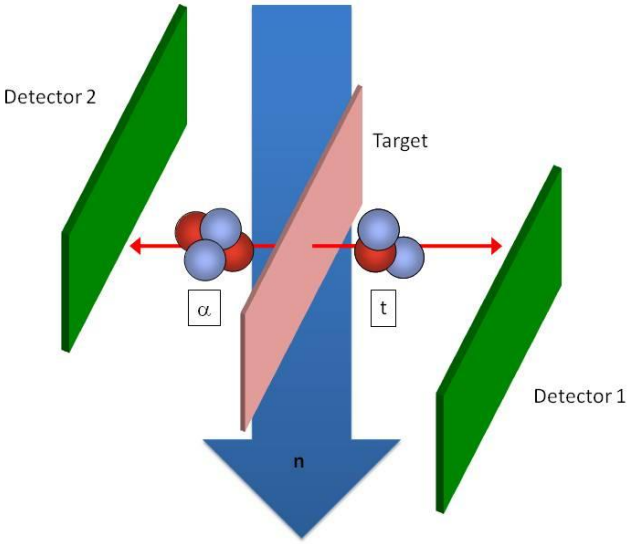

Figure 2.1: Schematic setup of the lithium detection [7]. The brain tissue (Target) is bombarded with thermal neutrons stimulating the decay of $^6\mathrm{Li}$.The decay products alpha and tritium are registered by two subtending detectors.

If an alpha and a tritium particle are detected simultaneously in the two detectors (coincidence condition) it is possible to trace back the trajectory and the initial position of the lithium atom can be located. The setup is calibrated with different calibration samples because the amount of particles that comply with the coincidence condition is position dependent, the neutron beam has an irregular profile and the geometric adjustment of the detectors and the target has to be factored in [8]. Taking into account that only 7.59% of lithium is $^{6}\mathrm{Li}$, it is finally possible to draw a map of the lithium distribution in the sample as shown in Figure 2.2 a), where the x and y axis are spatial coordinates in units of mm and the lithium density is color coded in units of $\mathrm{pg/cm^2}$. Thus, the experimental output is an areal density of lithium, however the desired result would be a spatial density. This is a particular matter of moment as the sample's thickness is most likely inhomogeneous due to fissures and deformations which is visible in Figure 2.2 b). In comparison with the histogram of the lithium distribution a correlation of thickness and areal density may be assumed in the black rimmed areas. Hence, in order to improve the accuracy of the results, the position resolved mass thickness of the tissue samples is determined in this bachelor thesis.

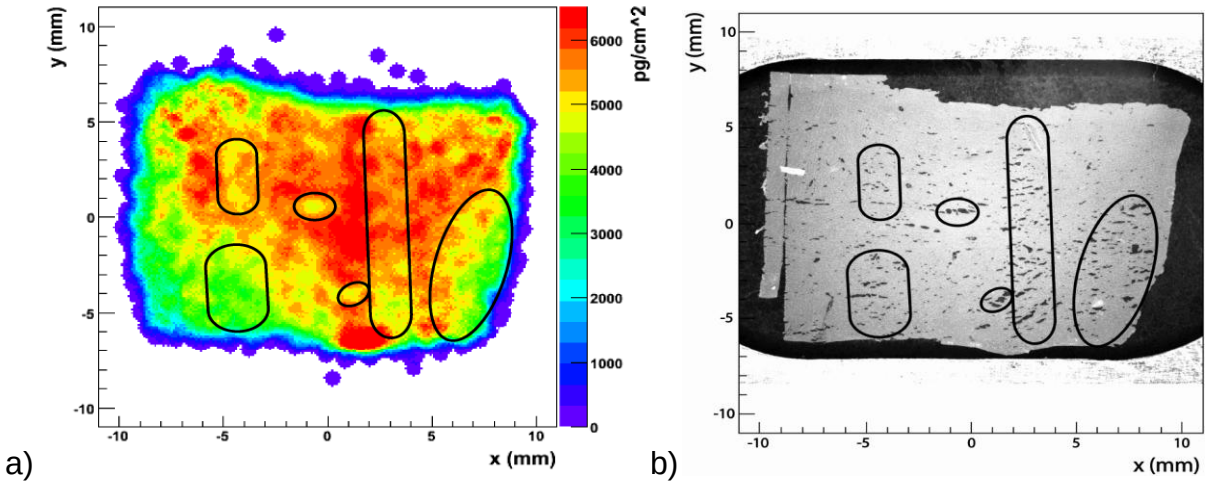

Figure 2.2: a) The lithium areal density of a brain tissue sample plotted against the position as a color map [7].
b) Picture of the corresponding sample from an optical microscope [7]. The black circles show pronounced structures visible on both sides.

2.2. Sample preparation

The properties of the brain tissue samples are essential for the lithium measurement as well as for the thickness measurement. Thus, it is important to understand the production process and the sample modifications introduced due to the different steps involved. The alpha and tritium particles have a rather high specific energy loss in solid matters. Therefore the samples have to be fabricated as thin as possible which consequently results in a loss of stability. As a reason of that, a holder with a stable foil substrate which carries the matter is constructed. In order to further reduce the amount of matter, the samples are freeze-dried.

2.2.1. Sample holder

The sample holder was special tailored to the requirements of the lithium experiment. It is a $30 \times 50\,\mathrm{mm}^2$ framework, crafted from a $0{,}2\,\mathrm{mm}$ thin super-purity aluminum plate with an elongated hole as shown in Figure 2.3 a). A cut-out at its bottom is used to center and fixate the samples.

This plate is covered with a polyethylene foil. It is extremely stretched to make it as thin as possible as the alpha particles will also have to pass this additional layer. Due to the stretching process the foil is altered. Firstly, it cannot be assured that its thickness is totally homogeneous and the 'Newton's rings' in Figure 2.3 b) provide an indication for that. Secondly, an electric charging of the foil may occur which may induce an increased accretion of dust on the surface.

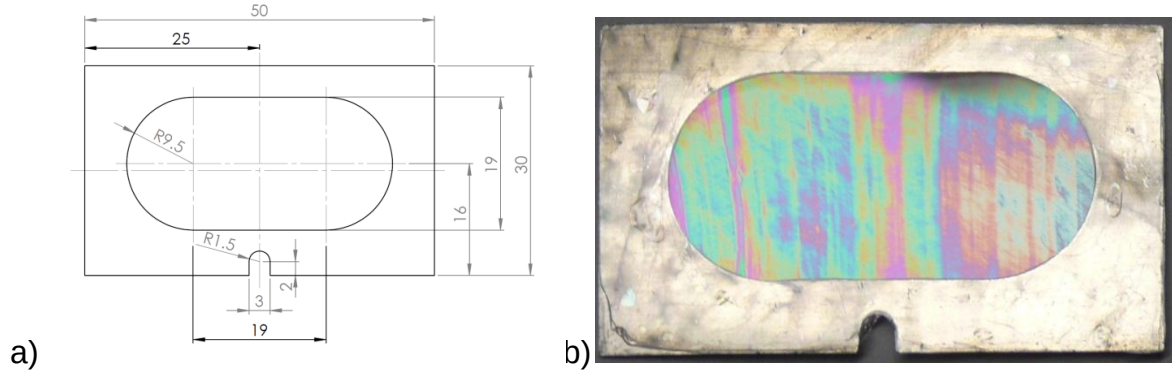

Figure 2.3: a) Design drawing of the sample holder with dimensions in mm [7]. b) The empty sample holder consists of an aluminum frame covered with a polyethylene foil. Colors indicate different optical thickness of the foil.

2.2.2. Sample fabrication

The organic matter for Josef Lichtinger's experiment is received from the forensic pathology of the Institut für Rechtsmedizin der LMU München[i], where the sample preparation was performed as well. The brain mainly consists of two different sorts of tissue, the white matter that contains mostly the nerve fibers and the gray matter, dominated by the cell bodies, the perikaryon [9]. Suitable tissue pieces of different regions in the brain are trimmed and frozen. They are thereafter installed into a microtome which is shown in Figure 2.4. The matter (1) is attached to a holder (2) that can be shifted down with a crank to cut the tissue with a blade (3) and up to move the tissue closer to that blade by a predefined value. The glass plate (4) prevents the sample from unfurling and can be lifted up to pick up the sample from the tray (5).

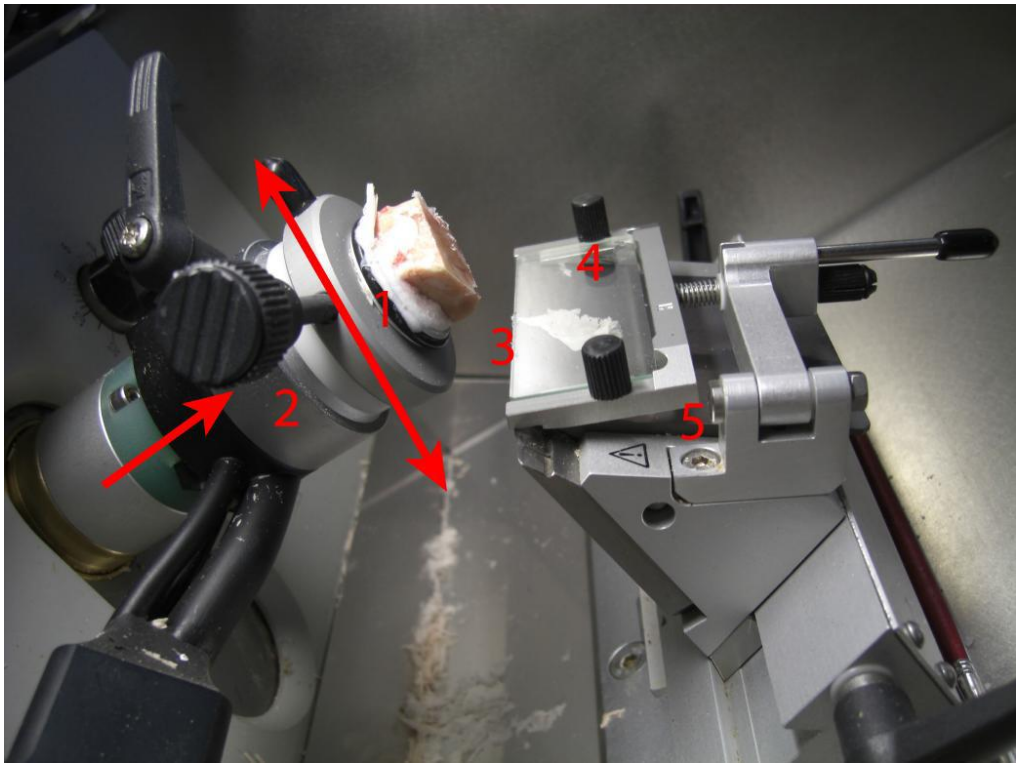

Figure 2.4: The interior of the microtome [7]. The tissue (1) is cut to 10 µm with the cutter (3). It is cooled to -20°C to prevent the deep frozen tissue sample from thawing.

It is possible to produce layers down to $1\ \mu m$ thickness, but even when using $10\ \mu m$ thick slices optimized for the lithium detection experiment, minor deformations, mainly in cutting direction, may occur. Moreover, due to temperature fluctuations a homogeneous thickness cannot be assured. Subsequently the tissue is put on the ready-made holders by laying the warm polyethylene film on the frozen cut. This step

[i] Nußbaumstraße 26, 80336 München

alters the sample the most, because while adhering themselves to the film they form a multitude of fissures and so the tissue is no longer distributed uniformly.

2.2.3. Freeze-drying

To further reduce the matter layer that the particles have to pass, the tissue samples are freeze-dried. For this, the samples are deep frozen by putting them on an aluminum block that was cooled to liquid nitrogen temperature and then put into a vacuum chamber. When the pressure drops below the vapor pressure of ice, the water crystals start sublimating from the tissue. In the lithium experiment it was measured that the samples lose approximately 78% of their mass during the drying [10]. The drying ensures a constant sample thickness during the lithium and thickness experiment as they are both performed inside a vacuum chamber at low pressure ($\mathrm{p} < 50 mbar$). Figure 2.5 shows a typical sample after all steps were performed.

Figure 2.5: Typical sample of brain tissue applied on a sample holder. The fissures in the tissue are clearly visible.

3. Thickness measurement with alpha particles

The production procedure of the samples has various effects on its thickness and so, even though the cutting is made with an extremely accurate microtome, it cannot be assured that the distribution of matter is still homogeneous on the final sample ready for measurement. As described in Chapter 2.1, in order to determine the spatial lithium density, the tissue's thickness profile has to be measured. Different technologies are available for that task and have to be evaluated with respect to the desired result.

3.1. Experimental method

One possibility to probe the sample's thickness is the mechanical scanning of the surface with a needle profiler. A similar but easier procedure is the optical survey of the sample, either by illuminating the sample and analyzing the interferences of the reflected light waves, or by focusing on the different depths with a microscope. Yet, these methods merely yield the elevation profile of the samples surface. However, the sample has a differentiated structure on both sides as illustrated in Figure 3.1. Even if executed on each side, air inclusions or other anomalies in the inside of the sample would not be taken into account. This would have severe impacts on the measurement results, as the amount of lithium correlates with the amount of mass of organic tissue. Thus, what is actually desired is not an optical thickness but a mass thickness of the tissue layer.

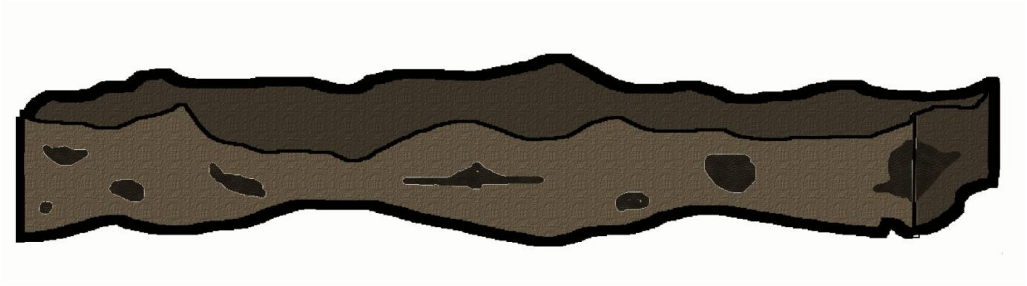

Figure 3.1: Schematic brain tissue layer. The upper and lower side both have a complex surface. Due to air inclusions or other anomalies in the sample (darker areas), conventional thickness determination methods do not yield the required mass thickness of the layer.

Consequently, another method is required that should be nondestructive and yields the mass thickness of the samples with a high spatial resolution. As the sample layers are fabricated thin enough so that they do not stop the alpha particles of the ^{6}Li decay, it is practicable to determine the sample thickness by the energy loss of

alpha particles. Therefore a setup as schematically shown in Figure 3.2 is used. Alpha particles from a point like source will penetrate the samples and are detected with a position sensitive detector. When passing through the sample the alpha particles lose energy by colliding with the atoms of the tissue and with the stopping power for alpha particles in organic tissue the desired mass thickness can be obtained.

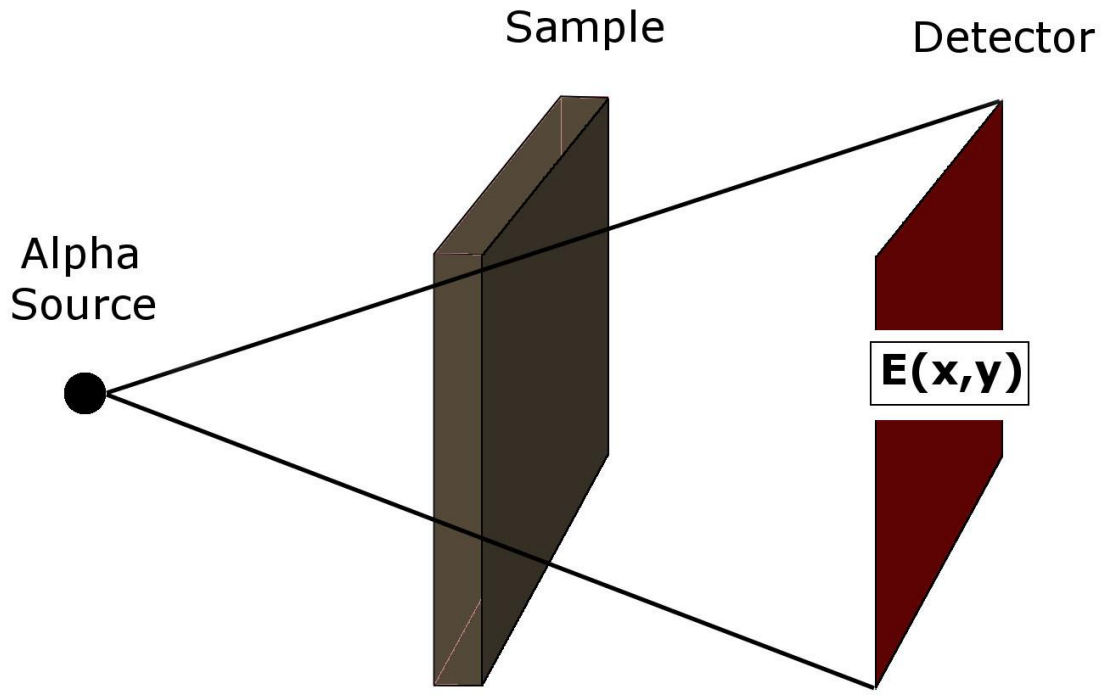

Figure 3.2: Schematic setup for the layer thickness determination. Mono energetic alpha particles from an $^{241}\mathrm{Am}$ source pass a thin layer of brain tissue before hitting a position sensitive detector. By the energy loss of the alpha particles and their specific stopping power in brain tissue, the thickness can be calculated.

It is necessary to place the setup in a vacuum chamber so that the alpha particles do not lose their energy in air. For the best possible resolution the total penetration depth of the alpha particles should be of the order of the layer thickness investigated. Hence, they should have an energy of approximately $2\,\mathrm{MeV}$ as the alpha particles' energy loss in the lithium experiment varied around up to $1{,}5\,\mathrm{MeV}$ [8]. However, there are no sources at such a low energy. Furthermore, it is crucial to use a single alpha source with a sharp peak to obtain a good energy resolution. The penetration depth of alpha particles in air is approximately $5\,\mathrm{cm}$ [11]. Therefore it is necessary to evacuate the measuring room where the alpha source is located.

3.2. Measurement setup

The layers thickness measurement is supposed to be integrated in the lithium experiment. Hence, the spatial resolution needs to be at least as good and the thickness resolution should not be lower than the lithium areal density resolution. In the following sections the different parts of the setup are described in detail.

3.2.1. Source parameters

The source used is a $^{241}\mathrm{Am}$ single alpha source with an energy of $5486\,\mathrm{keV}$, mounted into a fixture as shown in Figure 3.3 a). It is a closed alpha radiator with a diameter of $2{,}9\,\mathrm{mm}$ where the particles will have to pass the metalized foil, which broadens and also shifts the energy slightly. Figure 3.3 b) shows an energy spectrum from the source measured on a small area of a position sensitive detector (see Chapter 3.2.3) using the electronics described in Chapter 3.2.4. The distance between source and detector was $93\,\mathrm{mm}$ for this measurement. The root mean square deviation of a single alpha particle was measured to be $38{,}98\,\mathrm{keV}$. The energy resolution in the actual measurement is improved by a factor of $1/\sqrt{\mathrm{N}}$ for N incident alphas. Thus, it is important to have an alpha source with a high activity in order to get good statistics. In the used setup an average of 12 events per second were registered.

a) 

b) 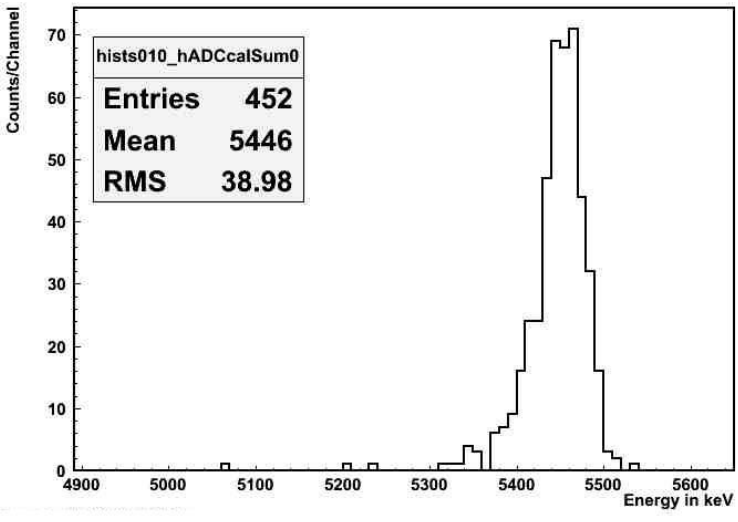

Figure 3.3: a) Retainer with alpha source. The $^{241}\mathrm{Am}$ is behind the metalized foil. b) Energy peak of the $^{241}\mathrm{Am}$ source measured on a small area of the PSD. The RMS for a single alpha particle is $38,98\,\mathrm{keV}$.

3.2.2. Detector setup

As shown in Figure 3.4, in front of the alpha source (1) the sample (2) and the detector (3) are positioned. Due to the alpha radiator not being ideally point shaped the measured particle positions on the detector plain do not directly correspond to unambiguous trajectories through the samples. At a finite distance ratio between source, sample and detector this introduces geometrical smearing. In order to minimize that additional error in position resolution, the distance between radiator and sample has to be large in comparison to the distance sample-detector. However the farther the detector is placed from the alpha source, the less alphas will reach there as the count rate drops with roughly $1/\mathrm{r}^2$. Therefore a compromise has to be found and in this setup the source - target and the target - detector distances used, are $89\mathrm{mm}$ and $3{,}0\mathrm{mm}$ respectively. With the alpha source diameter of $2{,}9\ \mathrm{mm}$, the geometrical smearing is calculated as follows:

$$\sigma_x = \sigma_y = \frac{2{,}9\mathrm{mm} \cdot 3{,}0\mathrm{mm}}{92\mathrm{mm}} = 0{,}095\mathrm{mm}$$

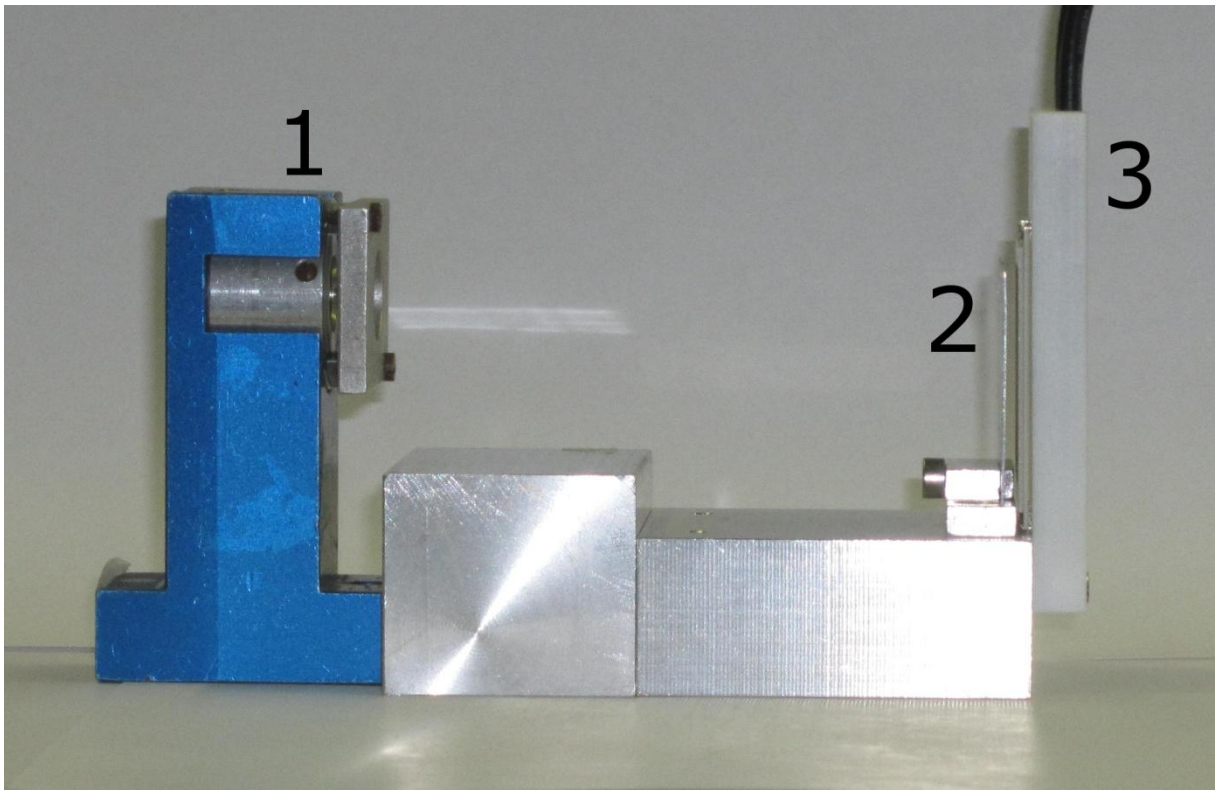

Figure 3.4: Side view of the setup in the vacuum chamber. The aluminum frame with the brain tissue (2) is placed 3 mm in front of the detector (3) and at a distance of 89 mm to the alpha source (1).

To implement these distances a mounting was designed to position the sample as close as possible to the detector. It is an aluminum block with a top part that centers the frames with the tissue in the same way as in the lithium experiment. This is important when the results of the two experiments shall be combined. At the end of the block the detector is installed (see Figure 3.4).
All parts shown in Figure 3.4 have to be placed inside a vacuum chamber in order to have constant measuring conditions. The chamber is evacuated down to a pressure below $\mathrm{p} < 10^{-5}\mathrm{mbar}$ using a fixed pumping station which combines roughing pump, turbo molecular pump and gauging cell in a single compact unit. The signals of the detector are transported through coaxial electric feed troughs to the outside electronics.

3.2.3. Detector

Figure 3.5 a) shows a front view of the position sensitive detector (PSD). Its internal structure is similar to a standard PIN-diode frequently used in particle physics and its active area is $20 \times 20\ \mathrm{mm}^2$ [12]. The silicon detector is mounted in a ceramic housing which is attached to a Teflon mount. An applied reverse voltage increases the space charge and makes sure that produced charges do not recombine before reaching the two contacts that are attached to each side of the detector (Figure 3.5 b) yellow stripes). The charge is split between the $\mathrm{x1}$ / $\mathrm{x2}$ and the $\mathrm{y1}$ /$\mathrm{y2}$ contacts respectively. The sum $\mathrm{x1} + \mathrm{x2}$ or $\mathrm{y1} + \mathrm{y2}$ correlates with the deposited energy and the incident location is obtained by calculating $\mathrm{X} = 10\mathrm{mm} \cdot \frac{\mathrm{x1}-\mathrm{x2}}{\mathrm{x1}+\mathrm{x2}}$. The scaling factor 10 is the half detector length and when repeating the calculation with the $\mathrm{y1}/\mathrm{y2}$ signals the Y-coordinate is obtained. On its front and back side, the detector has a capacitance of $360\mathrm{pF}$ and a resistance layer of typical $4\ \mathrm{k\Omega}$ between the two contacts of one side [12]. The four contact pads have zero resistance to their respective side. Therefore, the four analog signals are sensitive to the particle impact positions.

a)  b) 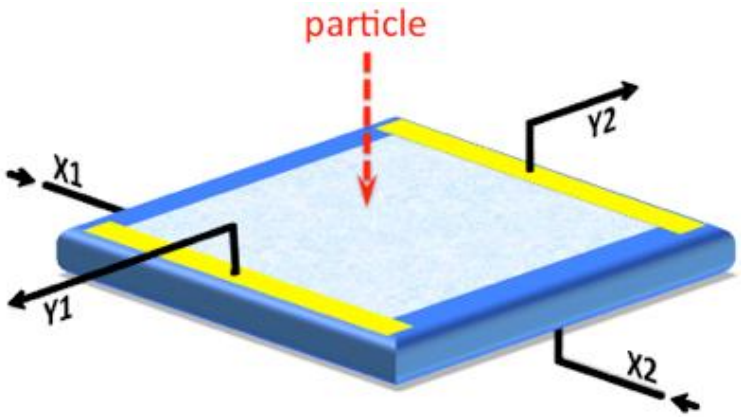

Figure 3.5: a) Position sensitive silicon detector used for the thickness measurement. The active area (black) is installed in a ceramic housing that is attached to a Teflon mount.
b) Schematic view of the detector [7]. An incident particle produces charge that is split between the two contacts (yellow) for both, the front and back side, yielding four signals (x1, x2, y1, y2). With the charge splitting the impact position is reconstructed.

The energy resolution of $\sigma_{\Delta E} = 38{,}89\ \mathrm{keV}/\sqrt{\mathrm{N}}$ was already introduced in Chapter 3.2.1. Using $5{,}5\ \mathrm{MeV}$ alpha particles, the spatial resolution of this detector has been tested to be $\sigma_x = \sigma_y = 124\ \mu\mathrm{m}$ **Fehler! Textmarke nicht definiert.**. Hence, combining this with the $95\ \mu\mathrm{m}$ error due to the used distances and source geometry, a spatial resolution of

$$\sigma_x = \sigma_y = \left(\sqrt{124^2 + 95^2}\right)\mu\mathrm{m} = 156\ \mu\mathrm{m}$$

is achieved in the thickness measurement. This is better by a factor of 2 in comparison with the lithium experiment where the resolution is $\sigma_x = \sigma_y = 300\ \mu\mathrm{m}$ because of a lower alpha energy.

3.2.4. Readout electronics

Figure 3.6 shows the readout electronics used in this setup. The four detector signals are amplified and shaped with a fixed shaping time of $2\ \mu s$ by a single MSI-8 module[ii]. It contains eight channels of preamplifier (PA), shaper and timing filter. Furthermore, a common timing signal is produced in the timing filter. The shaped and amplified

[ii] MSI-8, Mesytec (http://www.mesytec.de/)

signals are converted for the PC with an analog to digital converter[iii] (ADC). The timing signal is used to generate a trigger and to start the acquisition of the data. For that purpose it is converted to a digital signal with a leading edge discriminator[iv] (LED). This signal is also used to open a gate with a gate generator[v] (GG). The delay and width are adjusted relative to the discriminator signal so that the gate covers the peak of the shaped data signal. The gate is passed to the ADC which will only acquire data when the gate is open. Finally the data of all four channels are acquired synchronously event by event and transmitted to the readout software.

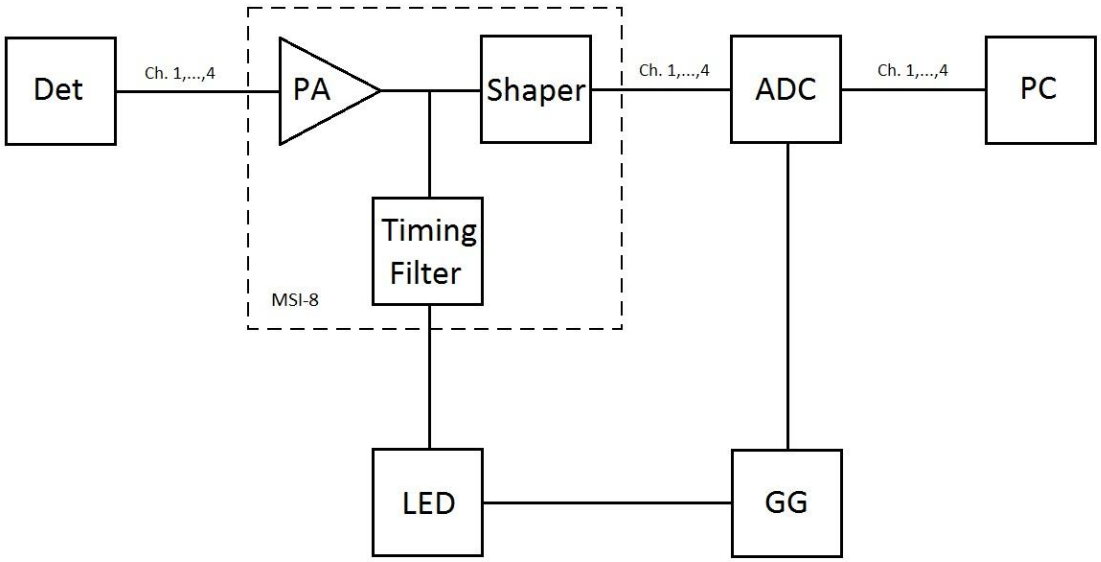

Figure 3.6: Schematic diagram of the data acquisition. In the MSI-8 module the four channels of the detector (DET) are amplified by a preamplifier (PA) and shaped. A common timing signal is produced and converted to a digital signal in a leading edge discriminator (LED) in order to open a gate with a gate generator (GG) and to trigger the data acquisition. The peak sensing analog to digital converter (ADC) will only acquire data and send it to a PC when the gate is open.

For controlling the data acquisition and collecting and processing the raw data, the software package MARABOU [13] is used. It also fills the processed data into histograms in an user defined way, while storing them into a so called 'root tree' based raw data file on disk. With each incident alpha particle the energy and hit position is calculated from the detector channels as described above. The number of impacts and the sum of the incident particles' energy is collected for each point of the detector plane. An extra macro is written to evaluate the average energy from this data and to calculate the energy loss and layer thickness (see Chapter 5.1).

[iii] V785, Caen (http://www.caen.it/)
[iv] Modell 708, Phillips Scientific (http://www.phillipsscientific.com/)
[v] Dual Gate Generator Model 222, LeCroy

4. Measurement calibration

Before the actual series of layer thickness measurements were started, all individual parts of the setup were calibrated and the stopping power of alpha particles in brain tissue was determined independently.

4.1. Electronics calibration

To calibrate the full electronics response for all four detector channels, a single $1 \times 1\mathrm{cm}^2$ silicon PIN-diode and a triple alpha source were used. The triple alpha source is a $380\ \mu\mathrm{m}$ thick mixture of $^{239}\mathrm{Pu}$ with an energy of $5157\ \mathrm{keV}$, $^{241}\mathrm{Am}$ with an energy of $5486\ \mathrm{keV}$ and $^{244}\mathrm{Cm}$ with an energy of $5805\ \mathrm{keV}$. The PIN-diode works in principal similar to the PSD, but shows a better energy resolution. This is due to the smaller area which corresponds to a smaller detector capacity, but also due to its smaller leakage current which is approximately $\mathrm{I} = 10\mathrm{nA}$. Moreover, it has only a single output signal which provides the full energy signal. Each channel of the ADC was calibrated one by one with the same signal. At first, the gain was adjusted to amplify the signal to roughly $1{,}2\ \mathrm{V/MeV}$ nicely fitting the ADC range. Then an energy measurement was performed and as the correct energies of the alpha peaks are well-known, the calibration factor was calculated with a linear fit. After repeating this procedure for each channel the alpha peaks were shifted to their right position in the linear spectra.

4.2. Detector calibration

For the calibration the single isotope $^{241}\mathrm{Am}$ source and the PSD were installed and an energy measurement was started. By using the PSD, the energy calibration did not completely match anymore. This is due to the resistance layers and the higher capacity of the PSD (see Chapter 3.2.3) in comparison to the single PIN-diode. Hence, the rise time of the detector signal, which correlates with $\sqrt{\mathrm{RC}}$ is position dependent. Charge produced in the middle of the detector sees a higher resistance and consequently has a slower rise time. If the rise time is not much smaller than the shaping time of $2\ \mu s$ a smaller energy signal is measured. Moreover, a fraction of the charge remains in the detector capacitance which further reduces the measured energy. These effects cause the bending of the histograms in Figure 4.1. On the left the color coded alpha particle counts are plotted against the energy ($\mathrm{E_x} = \mathrm{x1} + \mathrm{x2}$) and the X position ($\mathrm{X} = 10\mathrm{mm} \cdot \frac{\mathrm{x1}-\mathrm{x2}}{\mathrm{x1}+\mathrm{x2}}$) and on the right the same particle counts are plotted against the X and Y positions. The increased number of incident particles at the borders in the right picture are due to the zero resistance of the detector contact pads.

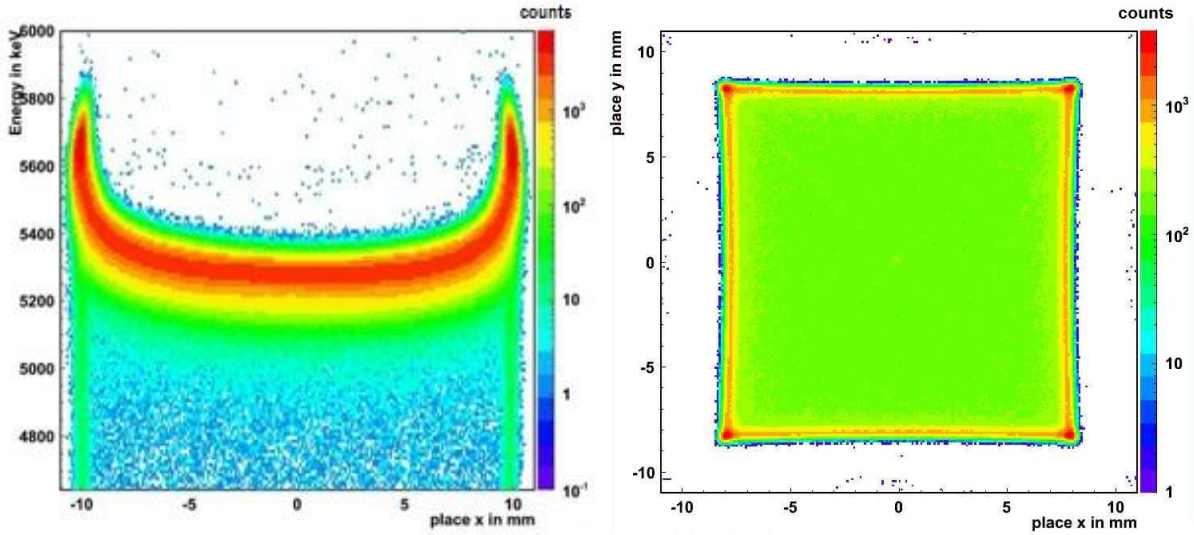

Figure 4.1: As the signal rise time of the four PSD signals correlates with $\sqrt{RC}$ the measured signal values are position dependent. The left histogram shows the color coded alpha particle counts plotted against the energy and the x position, the right one the same counts plotted against the x and y position.

The energy is bent around the true energy of $5486\,\mathrm{keV}$. To compensate for this effect, the bending was fitted and the histograms in Figure 4.1 got 'straightend', by dividing the initial space and energy values by those fits and thereafter multiplying them with the desired value. This is acceptable as the electronics effects dominates the energy shift caused by the thin foil of the closed single alpha source which is neglected in our analysis. The results are shown in Figure 4.2.

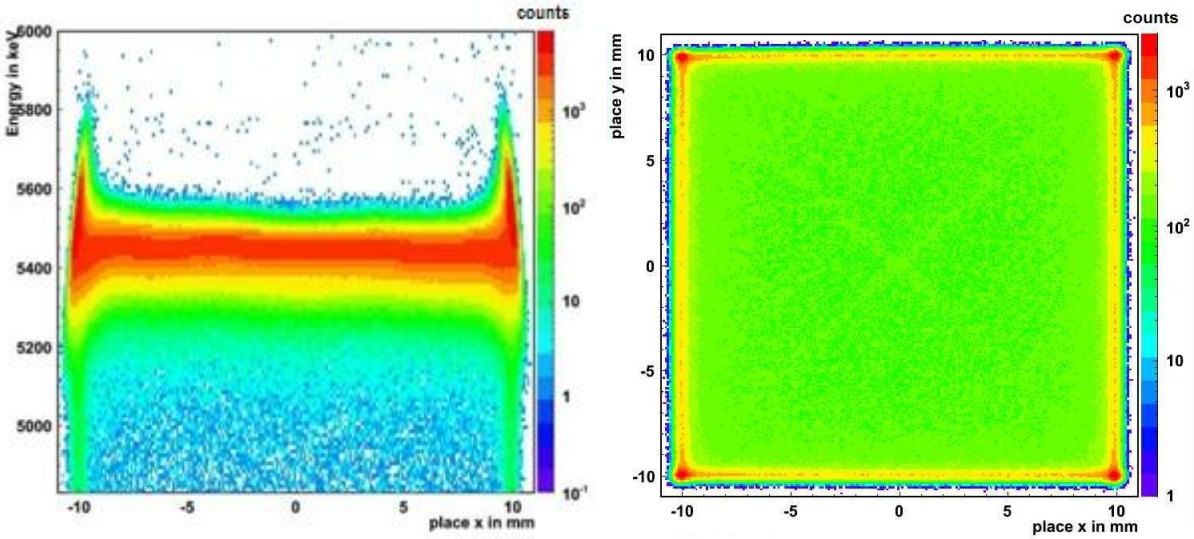

Figure 4.2: After fitting the bending, dividing the data by the fits and multiplying with the correct values, the data is now ready for further processing. This is acceptable as the bending and offset are predominantly caused by electronics effects.

4.3. Thickness calibration

It is necessary to determine the stopping power for the used brain tissue to calculate the layer thickness from the energy loss. The program SRIM [14] was used to simulate the energy loss for different layer thicknesses. By inserting the alpha particle energy, the layer composition, its thickness, and its density, SRIM will display the particle trajectory through the layer and the energy loss.

Hence, the chemical composition of brain tissue has to be known. 100g of an adults brain consists of 71,2g O, 14,5g C, 10,7g H, 2,2g N, 0,4g P, 0,3g Cl, 0,3g K, 0,2g Na and 0,2g S and has a density of $1{,}04\ \mathrm{mg/mm^2}$ [15]. This is merely the mass composition and needs to be converted to the stoichiometric ratio. Moreover, it is important to account for the 78% mass loss due to the freeze drying. Subsequently, the composition amounts to 56,1% H, 34,7% C, 4,5% N, 3,4% O, 0,4% P, 0,3% Na, 0,2% K, 0,2% Cl and 0,2% S. Next, the simulation was executed for different layer thicknesses of the above composition, yielding the data listed in Table 1. In Figure 4.3 the thickness is plotted against the energy loss and quadratically fitted:

Thickness d in µm	1	5	10	15	20	25
Energy loss ΔE in keV	91	466	954	1480	2054	2707

Table 1: SRIM simulation of energy loss in layers of different thickness

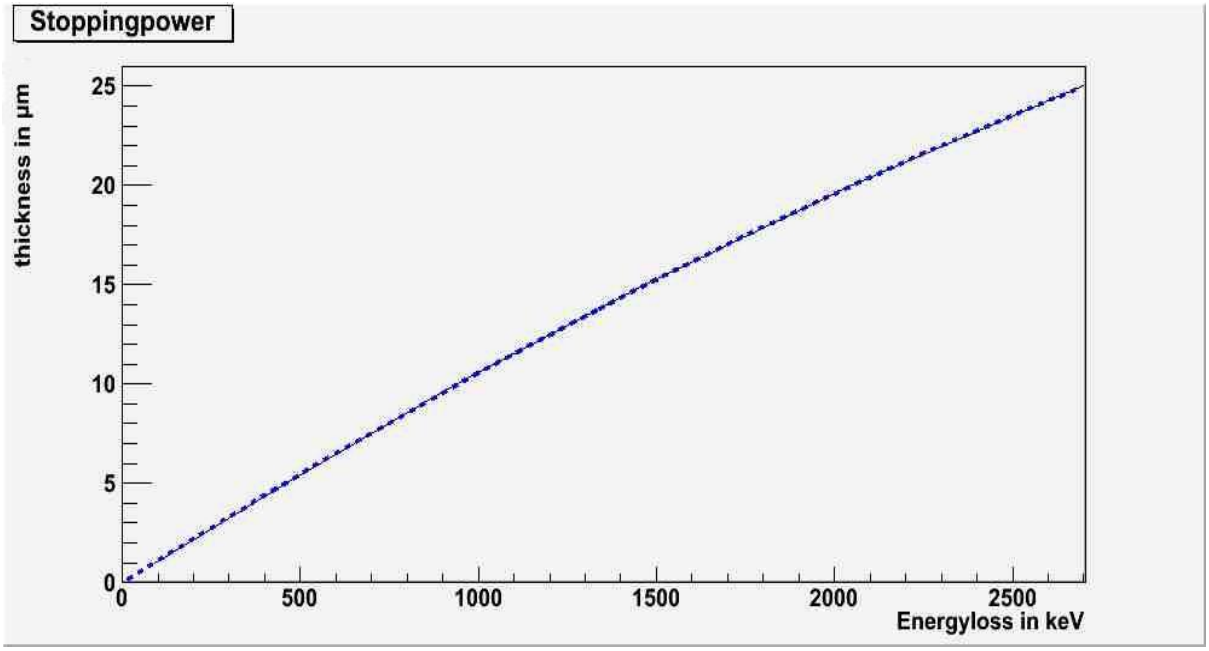

Figure 4.3: Quadratic fit of the SRIM data. The energy loss for different layer thicknesses was simulated.

The quadratic fit yields the thickness

$$\mathrm{d} = (-7{,}67 \cdot 10^{-7}(\Delta \mathrm{E}/\mathrm{keV} - 7{,}40 \cdot 10^{3})^2 + 41{,}9)\ \mu\mathrm{m}$$

Using that fit, the energy loss can be converted to the actual layer thickness. In this simulation the chemical properties between the substances was not considered. The stopping power in compounds differs up to 50% from the stopping power in the elemental matter that makes up the compounds [16]. This deviance applies especially for low-Z constituents as in the brain tissue. Moreover, the density inserted for the SRIM simulation, is the one of the original brain tissue since the density of freeze dried tissue was not known.
The SRIM simulation was also done with the foil material polyethylene, but this time a compound factor was taken into account. However, it yielded nearly the same result and consequently the above equation is used for both.

5. Experimental results and discussion

With the electronic part being calibrated the actual measurement series was started. The determination of the layer thickness is described in the following section. Moreover, additional measurements were performed in order to further investigate the properties of the brain tissue and to study the polyethylene foil's homogeneity. Additionally, a way of experimentally determining the stopping power is tested and compared with the SRIM simulation.

5.1. Measurement of the layer thickness

The determination of the layer thickness was performed for 49 samples that have been examined in the lithium detection experiment before. With a testing time of 2 hours and additional long-term measurements for specific samples, the measurement series covered a period of three weeks.

In the beginning no sample was installed and the energy of the alpha particles of the pure $^{241}\mathrm{Am}$ source was measured. The mean particle energy is calculated with a macro by dividing the energy sum with the number of impacts for each position on the detector. Figure 5.1 shows the mean energy plotted against the position as color map for the blank measurement. The average energy in the area between $\pm 9\mathrm{mm}$ in x- and y-direction is $5431\ \mathrm{keV}$. This is slightly less than the expected $5486\ \mathrm{keV}$ of the alpha particles. The reason for that are impacts with lower energy due to scattering at the mounting structure or PSD surface and can be partially seen in Figure 4.2 a) or Figure 3.3 b). Hence, without additional cuts the mean energy is reduced. But these cuts are not allowed in the later measurements as then, the lower energy of alpha particles will be caused mostly by the energy loss in the samples. Moreover, the measured energy decreased slightly over the three weeks. Three blank measurements were performed during that period, yielding mean energies of $5443\ \mathrm{keV}$, $5431\ \mathrm{keV}$, and $5426\ \mathrm{keV}$.

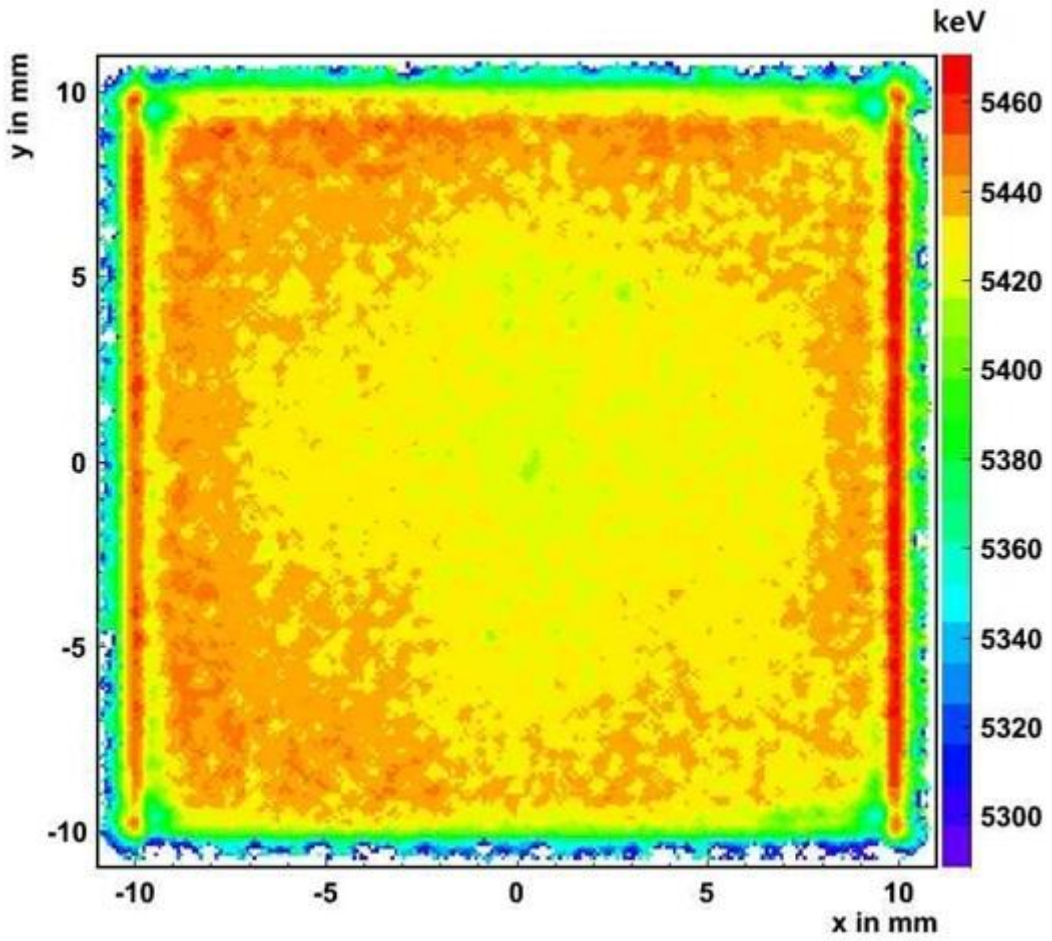

Figure 5.1: Mean energy measured with the PSD without sample and sample holder. Even though the setup was calibrated, the mean energy measured is lower than expected from the $^{241}\mathrm{Am}$ source and depends on the position on the PSD. Scattered alpha particles reduce the mean energy but they may not be excluded as the energy loss is measured with alphas at lower energies.

In the central active area of the detector the energy distribution is rather homogeneous and varies only between $5418\,\mathrm{keV}$ and $5428\,\mathrm{keV}$. As the position dependence of the energy measurement could not be completely removed by the calibration procedure described in Chapter 4.2, there is still a certain structure seen in Figure 5.1. In the border areas of the blank measurement there is a special profile which is due to the properties of the PSD's contacts (see Chapter 3.2.3) and hence, only the positions within $\pm 9\,\mathrm{mm}$ are considered in any calculations. All these are detector properties and thus, in order to obtain the energy loss, the average energy of a tissue sample is subtracted from the average energy of the blank measurement. In doing so, all systematic uncertainties of the PSD are canceled for the energy loss measurement. A typical result is shown on in Figure 5.2 where the color coded energy loss of the alpha particles is plotted against the position. The resolution of the energy loss is

$$\sigma_{\Delta E} = \sqrt{\left(\frac{38{,}98}{\sqrt{N_{sample}}}\right)^2 + \left(\frac{38{,}98}{\sqrt{N_{blank}}}\right)^2}\ \text{keV} \approx \frac{38{,}98}{\sqrt{N_{sample}}}\ \text{keV}$$

with N representing the number of incident particles for a random position bin in the blank and the tissue sample measurement. But as the measurement of the blank measurement was made over a period of 5 days, N_{blank} is certainly a lot higher than N_{sample}. Therefore the second term is neglected.

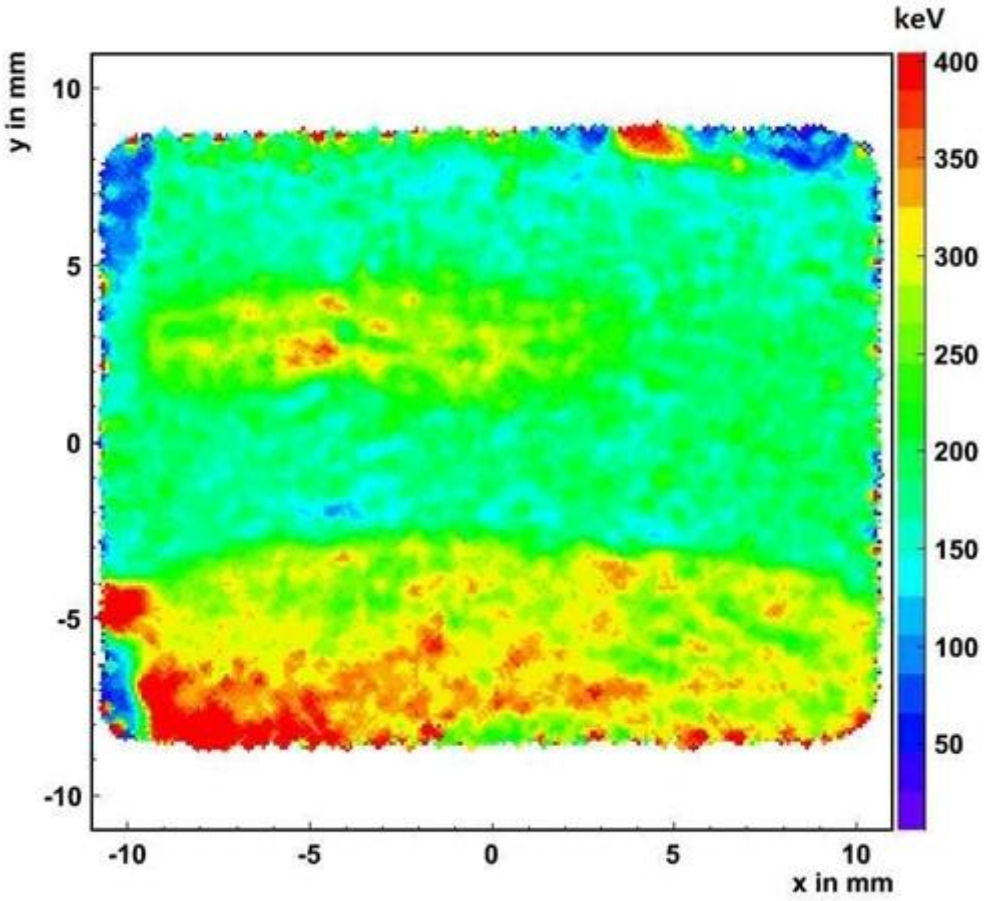

Figure 5.2: Energy loss of a typical tissue sample. The average energy loss was $226\ \text{keV}$. Clearly different regions are distinguishable. The energy loss in the bottom and middle area (yellow/red area) is roughly twice as high as in the rest (light blue/green area) of the sample.

Using the stopping power of the SRIM simulation (see Chapter 4.3), these energy loss histograms are transformed into layer thickness histograms. In Figure 5.3 two such histograms are compared with microphotographs of the respective tissue samples. The structure of the samples and even the fissures are clearly visible. The average thickness is $3{,}66\ \mu\text{m}$ for the upper and $3{,}38\ \mu\text{m}$ for the lower sample. With an average particle count of approximately 17 alphas per position bin, the uncertainty in thickness is $\Delta d = 0{,}08\ \mu\text{m}$. The mean layer thickness of the samples was calculated

for the whole series and is listed in Appendix 1. It roughly varies between $2{,}2\ \mu m$ and $4{,}2\ \mu m$, with only few exceptions. The calculated thickness still contains the polyethylene foil fraction of $0{,}9\ \mu m$ as discussed in Chapter 5.2.1. Hence, the mean tissue thickness is in the range of $1{,}3\ \mu m$ to $3{,}3\ \mu m$. Using the 78% mass loss due to the freeze drying [10] the initial thickness of the slices made, varied between $5{,}9\ \mu m$ and $15{,}0\ \mu m$. However, it is unclear whether the water loss due to the freeze drying is the same for every sample and for the different types of brain matter (see Chapter 2.2.2). In the second sample shown in Figure 5.3, the white brain tissue (brighter area in the microphotograph) has a higher mass thickness than the gray tissue. This matter needs further investigation and is discussed in the Outlook.

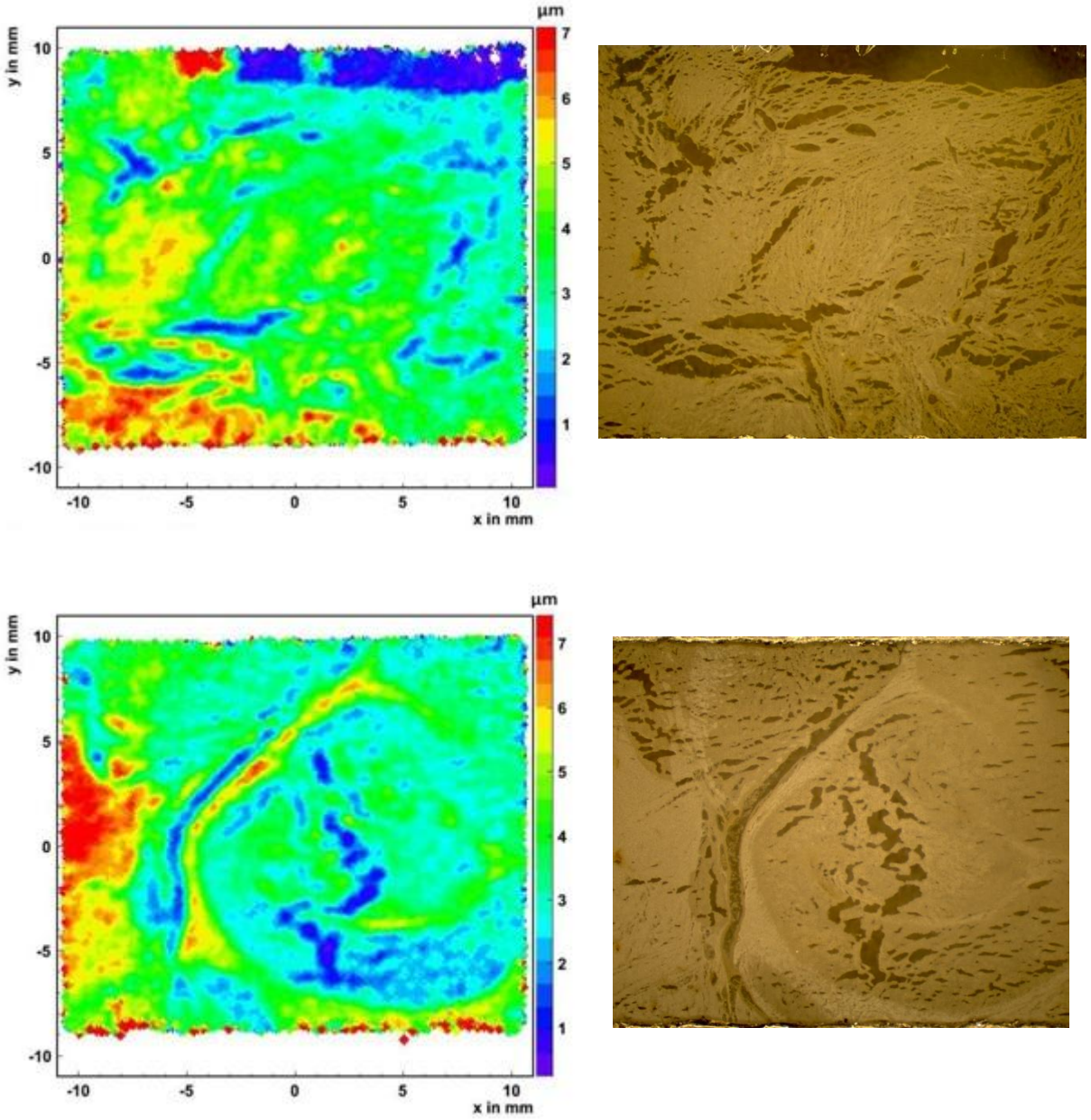

Figure 5.3: 2D representations of the layer thickness compared to the respective microphotographs for two different brain tissue samples. Even smaller structures of the samples are found in the histograms. The thickness ranges from approximately 1 µm (no tissue) to 7 µm.

The x and y coordinates shown in the histograms above do not exactly represent the real position. This is due to the position calibration in Chapter 4.2 and the optical enlargement of the setup. Therefore a layer thickness histogram with 50% opacity was put onto a microphotograph by visually aligning them (Figure 5.4). The lines on the microphotograph have well known distances and together with the histogram's scale, the x and y position are calibrated. The horizontal and vertical lines have a spacing of $18\,\mathrm{mm}$ and $14\,\mathrm{mm}$ respectively. Thus, $1\,\mathrm{mm}$ in the histogram translates into $0{,}88\,\mathrm{mm}$ on the sample surface.

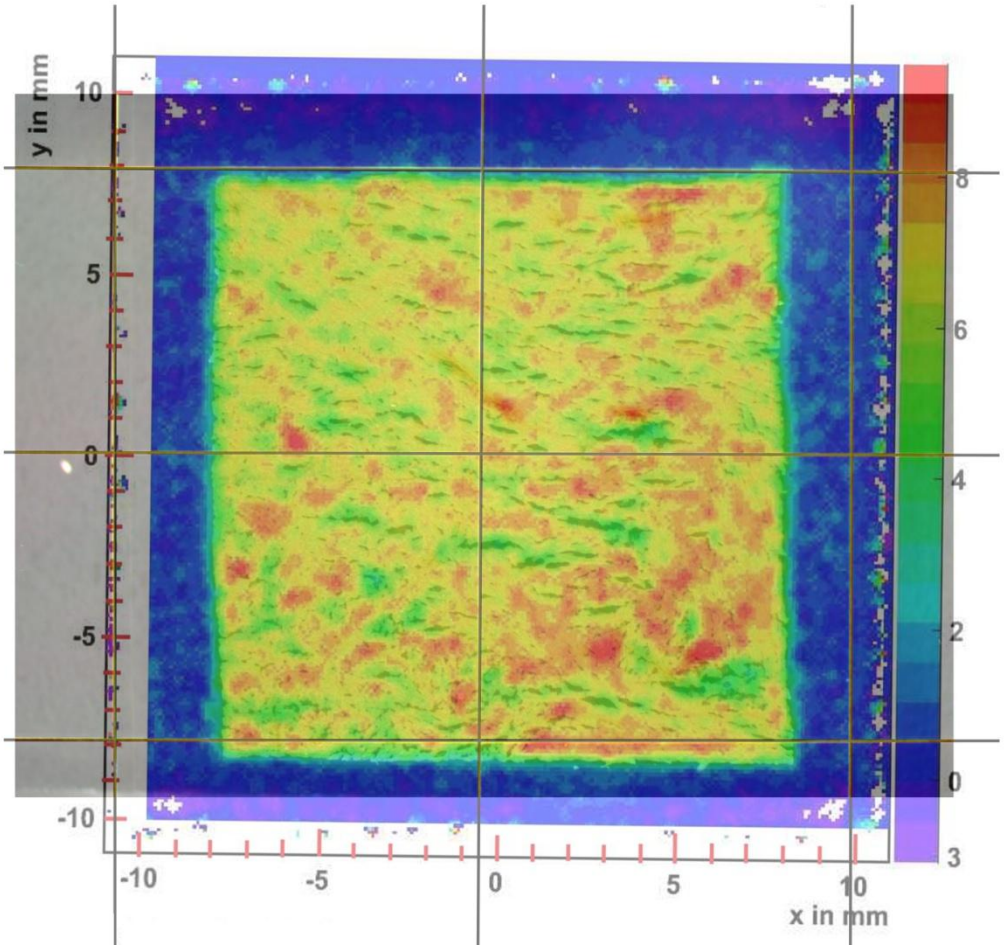

Figure 5.4: Layer thickness histogram with half opacity over the respective sample's microphotograph with threads of well-known distances on it. The two outer vertical lines are 18 mm, the two outer horizontal lines 14 mm apart. Combining the scaling of both axes results in 1 mm of the histogram corresponding to 0,88 mm in the microphotograph

5.2. Sample property measurements

In order to gain more information about the investigated samples, additional measurements were performed. The thickness of the polyethylene foil on which the tissue samples are applied was determined and tested for its homogeneity. Furthermore, the freeze drying process and its influence on the samples was observed.

5.2.1. Homogeneity of the polyethylene foil

In the layer thickness calculated in Chapter 5.1, the polyethylene foil is not subtracted yet. As it is supposed to be inhomogeneous (see Chapter 2.1), the foil is examined in more detail. For that purpose, layer thickness measurements with empty foils were performed (Appendix 2) as shown in Figure 5.5 for a single foil. To some extent, a structure resembling the color structure of the stretched foil is visible. Its average thickness is $1{,}30\,\mu\mathrm{m}$ with a root mean square deviation (RMS) of $0{,}38\,\mu\mathrm{m}$. The uncertainty in thickness caused by the energy resolution is only $0{,}04\,\mu\mathrm{m}$ and consequently it is assumed that the foil varies in thickness. A measurement with 5 foils installed in front of the PSD was performed and an average thickness of $0{,}89\,\mu\mathrm{m}$ and a RMS of $0{,}20\,\mu\mathrm{m}$ per foil was determined. This value has to be subtracted from the thickness measurements to gain the tissue thickness. Taking an average count of 30 alpha particles per bin the error in thickness amounts to $0{,}06\,\mu\mathrm{m}$. Hence, the fluctuations of the foil thickness cause an error of $0{,}19\,\mu\mathrm{m}$. This problem could be overcome by measuring all sample holders individually before attaching the tissue and then using them as reference measurements for the energy loss calculation instead of the blank measurement (see Chapter 5.1).

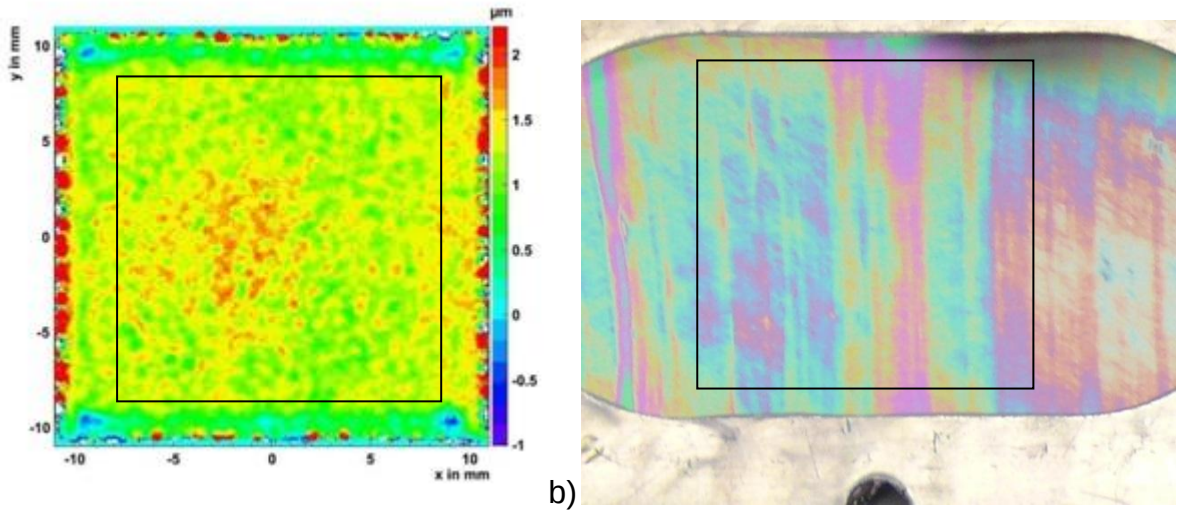

a) b)

Figure 5.5: a) Thickness measurement of a polyethylene foil without a tissue sample attached to it. The root mean square deviation of $0{,}38\,\mu\mathrm{m}$ was calculated for the black rimmed area. Fluctuations of the thickness between $0{,}9\,\mu\mathrm{m}$

and $1,7\ \mu m$ are visible and partially correlated with the black rimmed area of the photograph on the right.

b) Corresponding photograph of the polyethylene foil. The different colors were suspected to indicate regions of different optical thickness (see Chapter 2.2.1). In the area of the red stripe in the middle, the histogram shows a thinner foil thickness.

5.2.2. Tissue drying process

The drying of the tissue samples is unavoidable as the detector setup of the layer thickness measurement has to be placed inside a vacuum chamber (see Chapter 3.2.2) and the vapor pressure of water at room temperature is $23{,}4\ \mathrm{mbar}$. To study alterations of the sample due to the freeze drying, a sample before, after and during the drying was investigated.

Before evacuating the chamber to a pressure of $30\ \mathrm{mbar}$, a small bowl of water was put inside to keep the air humidity saturated and thereby slowing down the drying process as much as possible. Figure 5.6 a) shows the thickness measurement for the wet sample with the energy loss in the air already subtracted.

Next the water bowl was removed and a pressure of $250\ \mathrm{mbar}$ was applied and reduced in steps of roughly $50\ \mathrm{mbar}$ every 5 minutes. The steps were used to see the water reduction in the tissue at different pressures. In Figure 5.6 b) the alpha particle energy is plotted against the time. The energy gain (less water to pass through) is only observed in the first step ($250\ \mathrm{mbar}$). By pumping down to $180\ \mathrm{mbar}$ further drying could not be observed within the uncertainties of the measurement and the energy stayed constant over the 5 minutes. The steps observed are caused by the energy loss in the air that decreases by pumping down.

The layer thickness of the dried sample is shown in Figure 5.6 c). The average thickness of the wet sample is $(3{,}54 \pm 0{,}34)\ \mu m$ although it was cut to $10\ \mu m$. After the drying $(2{,}66 \pm 0{,}34)\ \mu m$ were measured. Assuming a $0{,}89\ \mu m$ foil the loss in thickness is $(33 \pm 5{,}3)\%$. However, the thickness should directly correspond to the mass which is supposed to decrease by 78% [10]. From the time dependent measurement (Figure 5.6 b)) it is suspected that while pumping down to the pressure of $30\ \mathrm{mbar}$, most of the water from the sample already started vaporizing and only small fractions remained in thicker structures.

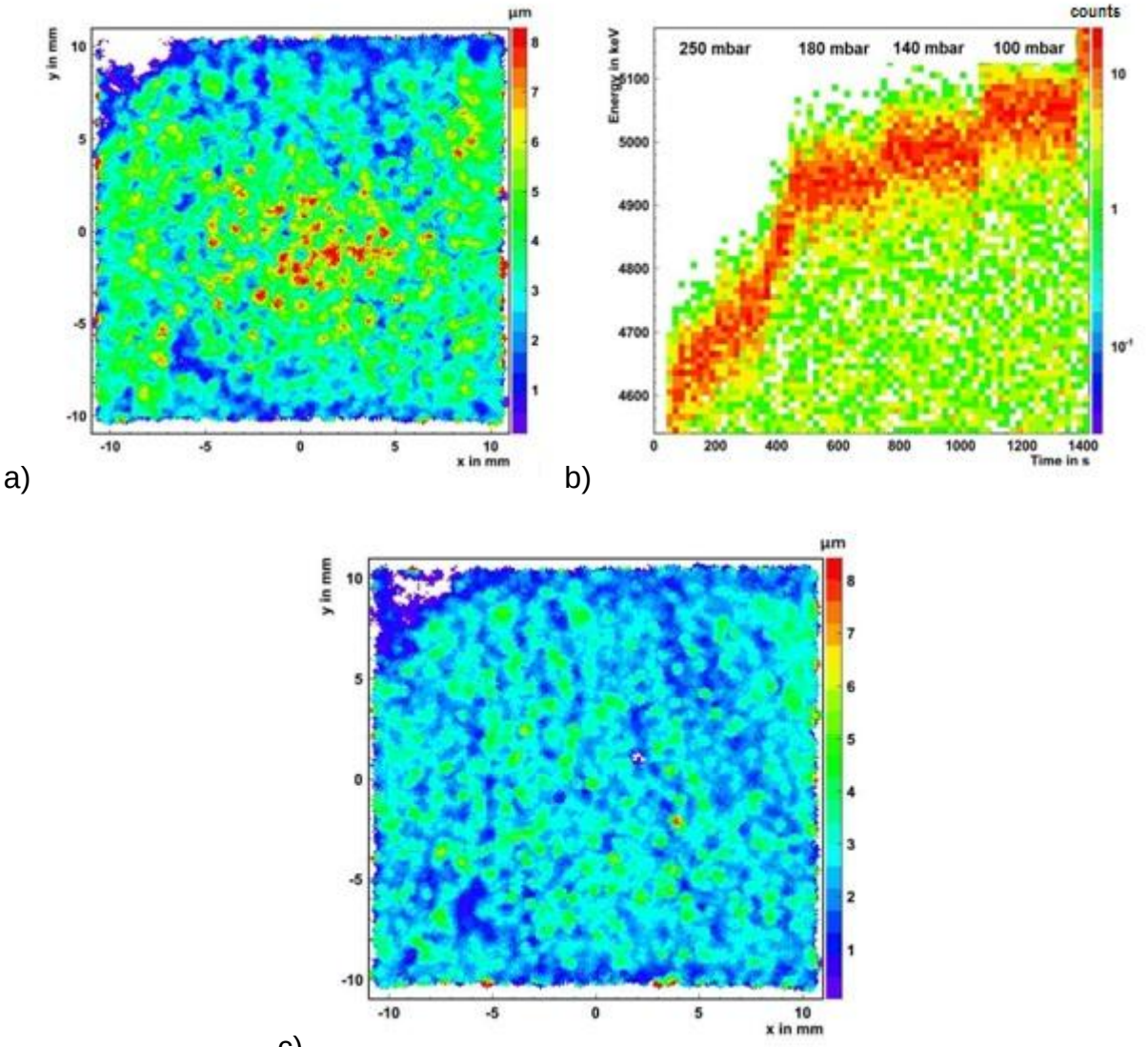

Figure 5.6: a) Layer thickness of a wet sample. During the measurement a pressure of $30\ \mathrm{mbar}$ was maintained. The additional thickness due to the air, is already subtracted. The mean thickness is $(3,54 \pm 0,34)$ µm.
b) Time dependence of the freeze drying. The energy of the alpha particles is plotted against the time for different pressures. The initial pressure was $250\ \mathrm{mbar}$ and was reduced in steps of roughly $50\ \mathrm{mbar}$ every 5 minutes. After the first step most of the water already vaporized. Hence, in the other steps only the pressure dependence of the energy is visible.
c) After completely drying at a pressure of $\mathrm{p} = 10^{-5}\ \mathrm{mbar}$ the sample has a mean thickness of $(2,66 \pm 0,34)\ \mu\mathrm{m}$. Most of the water was apparently lost in the central area.

5.3. Calibration of the specific energy loss in organic tissue

As described in Chapter 4.3, the SRIM calculation introduces an additional unknown error to transform energy loss into thickness and consequently, the reliability had to be tested with another experiment. The idea is to measure the energy loss of tissue samples of a specified area and a known mass. So it is possible to convert the energy loss histogram to a mass per area histogram. As the amount of lithium is specified in $\frac{\mathrm{pg}}{\mathrm{cm}^2}$ (see Chapter 2.1), the absolute concentration is obtained by dividing the lithium areal density by the mass areal density. This method of course does not require knowledge of the exact chemical composition and the density of the tissue. Furthermore, as the samples are fabricated the same way as those of the previous measurements, the obtained specific stopping power should be very reliable for a constant sample composition.

First of all new calibration samples were made. The brain tissue was cut to a $15 \times 15\mathrm{mm}^2$ square and layers of four different thicknesses were produced: 5µm, 10µm, 14µm, and 20µm. This was done for both, white and gray matter (see Chapter 2.2.2) in order to study the differences in the energy loss in those materials. The aluminum holders were weighed before and after the tissue was attached and freeze dried, in order to determine the weight of the tissue. However, the measured weight gain varied extremely and even took a negative value for one sample. Hence, the tissue mass had to be determined in a different way and the following procedure was found to yield the best results.

The calibration samples were weighed accurate to $0{,}1\ \mu\mathrm{g}$ before carefully removing the tissue with distilled water and isopropyl. After letting them dry for a few hours they were weighed again. The same procedure was performed for three empty holders to determine the error due to removed dirt or other effects. The mass change is listed in Table 2. Assuming an average mass change of zero for the reference samples, the standard deviation is $16\ \mu\mathrm{g}$ which is less than 6% of the weight of the lightest calibration sample. As this method destroys the samples weighing cannot be repeated with the same sample.
The mean energy loss listed in Table 2 was calculated from a $251\ \mathrm{mm}^2$ area that completely covered the tissue samples.

Sample	5µm white	10µm white	14µm white	20µm white	Reference	Reference
$\Delta\mathrm{m}$ in mg	0,5563	0,7759	1,1024	1,3822	-0,0098	0,0186
$\Delta\mathrm{E}$ in keV	228	310	410	517	-	-
Sample	5µm gray	7µm gray	10µm gray	14µm gray	Reference	-
$\Delta\mathrm{m}$ in mg	0,2785	0,3746	0,6424	0,9147	-0,0075	-
$\Delta\mathrm{E}$ in keV	141	161	277	369	-	-

Table 2: Weight measurements of the 'calibration' samples

In Figure 5.7 the mass per area ($\Delta m/251 mm^2$) is plotted against the energy loss for the white and for the gray brain matter. For both types a linear correlation with rather similar slope and offset are visible.

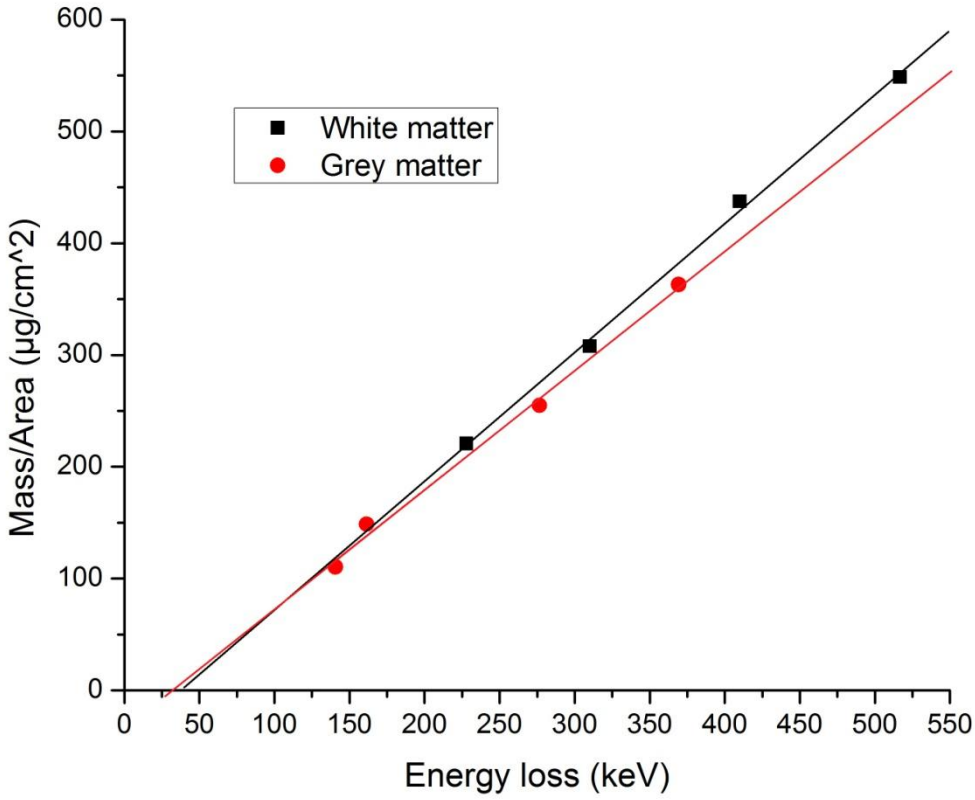

Figure 5.7: The mass of a fixed area of tissue is plotted against the energy loss. The slope is the specific stopping power and is for both types of brain tissue consitent within the uncertainties.

The fits yielded the thickness

$$D_w = ((1{,}152 \pm 0{,}036)\Delta E/\mathrm{keV} - (42{,}957 \pm 13{,}683))\frac{\mu g}{cm^2}$$

for white tissue and

$$D_g = ((1{,}064 \pm 0.052)\Delta E/\mathrm{keV} - (32{,}871 \pm 13{,}312))\frac{\mu g}{cm^2}$$

for gray in which ΔE is the energy loss. Within the uncertainties the results are consistent and thus, an identical stopping power for both materials is assumed. The combination of both data would be used anyways as the actual brain tissue examined in the lithium experiment is always a composition of white and gray matter. The offset is a result of the additional energy loss in the polyethylene foil. Thus, the x-intercept of $(41{,}509 \pm 9{,}695)\mathrm{keV}$, calculated for the combination of the data, yields

the mean energy loss in the foils of the calibration samples. This relates to an average foil thickness of $(0{,}45 \pm 0{,}09)\mu\mathrm{m}$ which is only half of the one determined in Chapter 5.2.1. Considering the foil thickness variability also discussed in that section the uncertainties of the slopes are most likely introduced by them.
In a next step, the difference between this calibration and the SRIM simulation is investigated. Figure 5.8 shows the mass per area plotted against the energy loss for both, simulation and experiment.

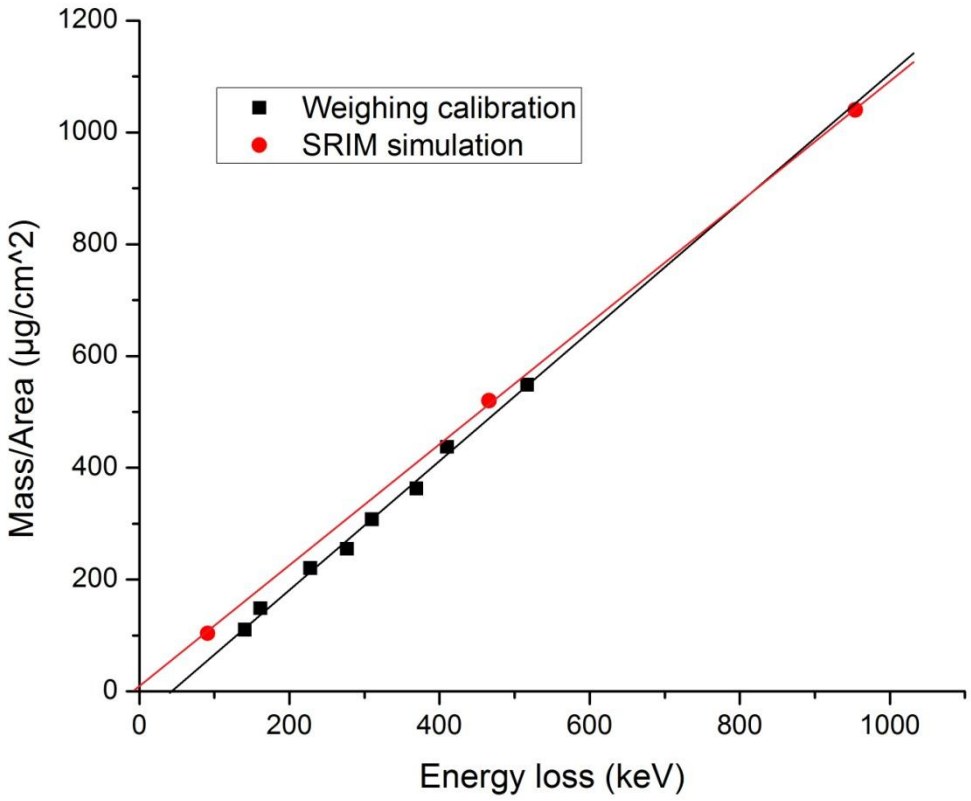

Figure 5.8: The slope yields the specific stopping power of the calibration and the SRIM simulation. The energy loss in the polyethylene foil is included in the weighing calibration but not the SRIM simulation and thus has to be factored out.

Here the fit was made with the white and gray tissue together and yielded:

$$\mathrm{D_{calib}} = ((1{,}149 \pm 0{,}034) \cdot (\Delta\mathrm{E})/\mathrm{keV} - (47{,}694 \pm 11{,}050))\frac{\mu\mathrm{g}}{\mathrm{cm}^2}$$

The fit for the SRIM simulation is

$$\mathrm{D_{SRIM}} = ((1{,}084 \pm 0{,}012) \cdot (\Delta\mathrm{E})/\mathrm{keV} + (8{,}866 \pm 7{,}595))\frac{\mu\mathrm{g}}{\mathrm{cm}^2}$$

To obtain the total uncertainty in thickness the energy resolution $\sigma_{\Delta E} = \frac{38{,}98}{\sqrt{N}}$ (see Chapter 5.1) has to be factored in. The slope of the weighing calibration derivates from the SRIM simulation's slope by $6{,}0\%$. They do not match within the uncertainties, but as the specific stopping power calibration is supposed to be more accurate, it can be used to analyze the measured series and further samples.

In Figure 5.9 a) this was done for a single sample. The layer thickness in units of $\mu g/cm^2$ is plotted against the position. The white area is due to the foil thickness being included in the specification of the stopping power. Figure 5.9 b) shows the respective microphotograph.

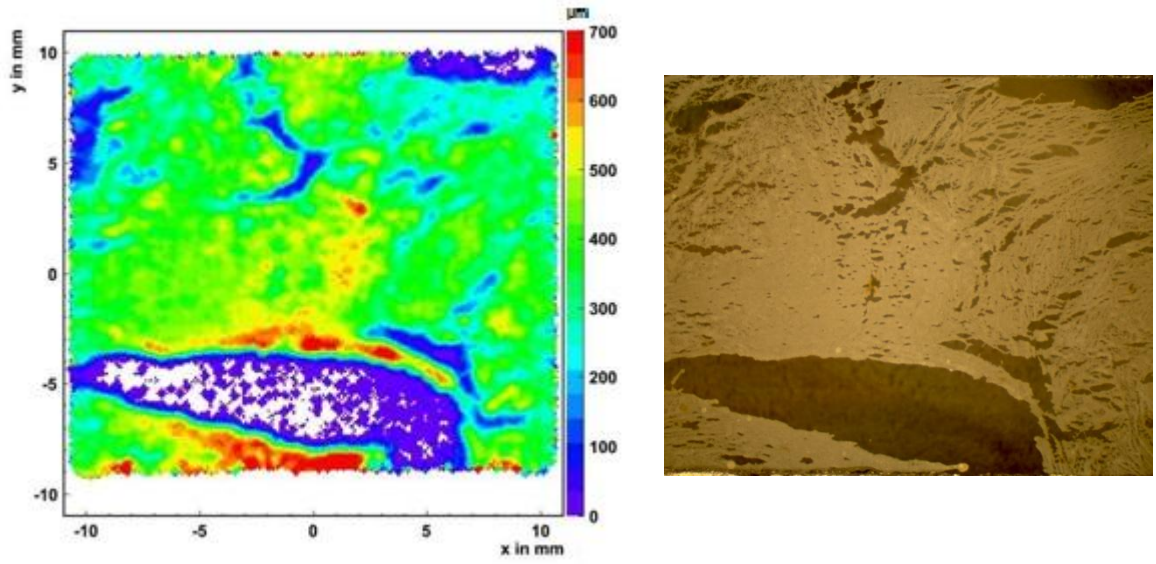

a) b)

Figure 5.9: a) Layer thickness calculated with the specific stopping power gained from the energy loss per mass per area. The thickness is specified in $\mu g/cm^2$. The white area is due to the foil thickness being implemented in this stopping power calibration
b) Respective microphotograph. The foil in the area without tissue is only approximately $45\ \mu m$ thick.

6. Outlook

In this bachelor thesis it was possible to determine the thickness of 49 brain tissue samples with a spatial resolution of $156\,\mu m$. For a typical sample of $3{,}5\,\mu m$ thickness (including the foil thickness) and a mean alpha particle count of 17 per position bin (corresponding to a energy resolution of $\Delta E = 9{,}45\,keV$), the relative thickness uncertainty is 5% if calculated with the specific stopping power calibration and $2{,}4\,\%$ if done with the SRIM simulation's stopping power. The seemingly worse resolution of the calibration is due to the unknown uncertainty introduced by the SRIM simulation that is supposed to be a lot higher. Hence, the already measured series of tissue samples needs to be converted with the specific stopping power calibration.
The next step is to combine these results with those from the lithium experiment. By dividing the lithium areal density by the mass areal density, the absolute lithium concentration of the examined tissue (and thereby brain region) is obtained. However, it is not clear whether all samples were installed in exactly the same position. Furthermore, due to the different setups of both experiments, the position calibration may vary and thus, a way of correctly combining the measuring data must be figured out. Putting well visible landmarks on the samples that are detected in both experiments could be a feasible approach. With these landmarks it is possible to calibrate both measuring data to match each other.
Moreover, the lithium concentration determined with the method above, is the one of freeze dried brain tissue. To obtain the concentration in the original tissue, it should merely be necessary to take the 78 % mass loss during the freeze drying [10] into account. However, in this bachelor thesis indications were found that the mass loss of white and gray tissue differ from each other. As described in Chapter 5.1 with regard to Figure 5.3, it seems as if the white brain tissue has a higher mass thickness than the gray tissue But as both were cut to $10\,\mu m$, the mass loss during the freeze drying has to be the decisive factor. Apparently, the gray matter contains more water than the white. Another indication for that is the calibration samples (see Chapter 5.3) of the white tissue being heavier than those of the gray tissue, though both were cut to the same thicknesses. Hence, to obtain the lithium concentration of the original brain tissue, it is required to determine the mass loss during the freeze drying for both types of tissue.

Another factor that has to be considered is the polyethylene foil's thickness as discussed in Chapter 5.2.1. In Appendix 2 the mean foil thickness is listed for different empty holders and it is evident that they vary a lot. Moreover, the mean thickness calculated from 5 such holders was measured in Chapter 5.2.1 to $0{,}89\,\mu m$ whereas in Chapter 5.3 the x intercept of the specific stopping power fit yielded a mean foil thickness of $0{,}45\,\mu m$. Varying so much, it is very important to find ways of better controlling the foil's influence on a thickness measurement. A way of doing so, could be to measure the energy loss in the sample holders before the brain tissue is

deposited (or after it is removed for the calibration samples) and to use that one as the reference measurement instead of the blank measurement (see Chapter 5.1).

The setup of the thickness measurement could be improved by using a single alpha source with a higher activity but smaller active area, as the additional position uncertainty discussed in Chapter 3.2.3 would diminish. But more importantly, the measuring time is determined by the amount of incident alpha particles, as that controls the energy resolution (see Chapter 5.1) and as there should be at least one particle per position bin. The histograms shown above are mostly from long-term measurements which needed a period of approximately 16 hours and had a average count of 17 alpha particles per position bin. Samples that were measured for only 2 hours however had a average count of 2 and consequently show a much worse resolution as shown in Figure 6.1.

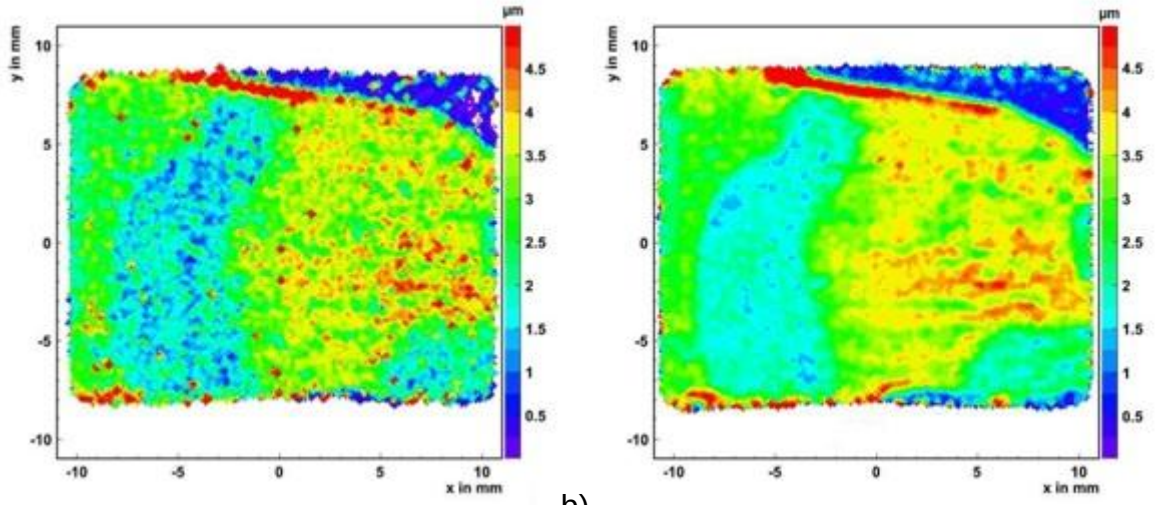

a) b)

Figure 6.1: a) Layer thickness for a measuring time of $2\ \mathrm{h}$.
b) Same sample but with a measuring time of $16\ \mathrm{h}$. The resolution has clearly improved.

Another way to get more incident particles is to position the alpha source and the detector closer to each other. The pretense for the spatial resolution was to be at least as good as the lithium experiment's, which translates into an upper limit of $300\ \mu\mathrm{m}$. Additionally, with an improved setup, it would be possible to put the sample $1\ \mathrm{mm}$ in front of the detector. Considering the spatial resolution of the detector $\sigma_x = \sigma_y = 124\ \mu\mathrm{m}$ and the alpha source diameter of $2{,}9\ \mathrm{mm}$ the distance between detector and source could be reduced to

$$x_{\mathrm{det}-\alpha} = \left(\frac{2{,}9 \cdot 1}{\sqrt{0{,}3^2 - 0{,}124^2}} - 1\right)\mathrm{mm} = 9{,}6\mathrm{mm}.$$

In comparison with the used distance of $93\ \mathrm{mm}$ the number of incident alpha particles would be approximately 2 orders of magnitude higher. Consequently, a 17 hours measurement's result could be obtained in roughly 10 minutes. However, the closer the source is located to the sample the higher the possible inclination of alpha particles passing through the samples, which consequently results in a higher energy loss. Moreover, those alphas will no longer be a direct measure for the desired mass thickness but one depending on the angle of impact. In addition, the dead layer of the detector introduces a further systematic error and together with the large area of the source also a statistical error. It is a matter of further investigation to determine the optimal distance.

Appendix

#1

Sample	Measuring time in s	Average energy loss in keV	Average thickness in µm
C03	9300	315,8	3,4615
C04	7285	270,971	2,98927
C05	7340	312,497	3,42778
C07	54889	306,915	3,37636
C14	7304	231,106	2,55112
C15	7300	259,946	2,85976
C17	61373	312,915	3,45002
C18	61318	332,898	3,66458
C27	8205	288,934	3,1824
C28	7300	288,784	3,17421
A28	6555	248,627	2,74286
A28	58517	261,725	2,89808
A43	52201	226,302	2,50315
A46	242407	378,195	4,15346
A108	6700	334,143	3,63596
A109	8894	263,88	2,9015
A114	57149	200,958	2,21615
A117	7938	215,848	2,38331
A200	7455	284,4	3,12487
A201	7000	242,167	2,66024
A202	7200	284,723	3,14179
A203	9161	291,616	3,20639
A204	7099	334,761	3,67979
A205	7650	352,922	3,87777
A206	67959	311,637	3,44074
A207	6951	776,97	8,21558
A208	55451	553,884	6,02375
A210	7207	269,451	2,94887
A211	7080	307,778	3,38402
A212	7120	274,79	3,02753
A213	7140	280,127	3,09127
A214	7201	369,769	4,0494
A215	7200	210,495	2,32338
A216	7229	358,069	3,92581
A217	7210	261,805	2,89414

A218	7300	315,56	3,46105
A219	7218	355,116	3,89345
A220	7700	319,558	3,51557
A221	7200	339,123	3,72674
A222	7236	299,608	3,29443
A223	7201	406,398	4,44635
A224	7204	311,255	3,42405
A225	7080	318,723	3,51253
A226	7035	270,66	2,97716
A227	7287	287,545	3,16176
A228	7447	297,9	3,2819
A229	52659	290,955	3,21065
A230	7653	369,889	4,05625
A231	7204	341,97	3,75355

Table 3: Layer thickness measurement of the brain tissue samples

#2

Sample	Measuring time in s	Average energy loss in keV	Average thickness in µm	RMS in µm
A8	242782	116,92	1,29483	0,3766
A10	74192	102,118	1,12059	0,5047
T6	68536	94,4754	1,04327	0,5112
T7	10331	59,3027	0,616143	0,6123
A5,A9	7652	161,045	1,69801	0,6194
A5,A8, A9,T6,T7	63770	391,973	4,3141	0,4381

Table 5: Layer thickness measurement of empty holders

#3

Sample	Measuring time in s	Average energy loss in keV	Average thickness in µm
A13w	9135	903.71	6,51367
A13d	8437	480,348	5,2075
T2w	9360	584,204	3,33325
T2d	8706	244,248	2,65779

Table 4: Layer thickness measurement of wet and dried tissue samples

Bibliography

[1] Ayuso-Mateos, J.L. et al.: Depressive Disorders in Europe: Prevalence Figures from the ODIN study. British Journal of Psychiatry (2001)

[2] Thomas Köhler: Medizin für Psychologen und Psychotherapeuten: Orientiert an der Approbationsordnung für Psychologische Psychotherapeuten. 2nd ed., Schattauer (2010)

[3] Abell, S.; Ey, J. L.: "Bipolar Disorder". *Clinical Pediatrics* (4 June 2009)

[4] Claus-Jürgen Estler, Harald Schmidt: Pharmakologie und Toxikologie. 6th ed., Schattauer (2006)

[5] Josef Lichtinger: Spurenelementnachweis von Lithium in organischem Gewebe mit Neutronen, Psi-seminar (2012)

[6] J. Blatt, V. Weisskopf: Theoretische Kernphysik. Teubner (1959)

[7] Picture by Josef Lichtinger

[8] Josef Lichtinger: Spurenelementnachweis von Lithium in organischem Gewebe mit Neutronen, Diploma thesis (2010)

[9] Purves, Dale, George J. Augustine, David Fitzpatrick, William C. Hall, Anthony-Samuel LaMantia, James O. McNamara, and Leonard E. White. *Neuroscience. 4th ed.*. Sinauer Associates (2008)

[10] Experimental results of Josef Lichtinger

[11] Shatendra Sharma: Atomic and Nuclear Physics. Dorling Kindersley (2008)

[12] Data Sheet: High Linearity Position Sensing Detector, Part Numbe:r S2-0034, Description: 2L20UV_SU9. Laser Components

[13] R. Lutter, O. Schaile, K. Schöffel, K. Steinberger C. Broude : MBS and ROOT Based Online Offline Utility (http://www.bl.physik.uni-muenchen.de/marabou/html/)

[14] Stopping and Range of Ions in Matter, ver.SRIM-2008.04 (www.SRIM.org)

[15] ICRU: Photon, Electron, Proton and Neutron Interaction Data for body tissues. International Commission on Radiation Units and Measurements (1992)

[16] D.I. Thwaites: Bragg's Rule of Stopping Power Additivity: A Compilation and Summary of Results. Radiation Research (1983)

Danksagung

Zu aller erst möchte ich Herrn Prof. W. Henning danken, der dieses spannende Thema stellte und mir damit zu dieser Arbeit verhalf.

Außerdem bedanke ich mich bei meinem Betreuer Dr. R. Gernhäuser der mich mit fachkundigem Rat durch die letzten drei Monate geleitet hat und mir da mit Wissen zur Seite stand wo es bei mir noch fehlte. Mit seiner konstruktive Kritik half er mir meine Arbeit immer weiter zu verbessern

Besondere Dank gilt auch Josef Lichtinger, dessen Doktorarbeit den Rahmen dieser Arbeit darstellt und der mir stets mit Rat und Tat zur Seite stand. Er versorgte mich mit dem nötigen Wissen über seine eigene Arbeit und half mir zielgerichtet an ihrer Verbesserung mitzuwirken.

Auch bedanken möchte ich mich bei dem Rest des E12 Teams und dem Werkstattteam für ihre Hilfsbereitschaft und der Fertigung meiner Halterung.

Schließlich noch ein großes Dankeschön an Frederik Schönebeck für seine hilfreiche Korrekturlesung und an meine Freunde und Familie, die mich immerzu unterstützt und motiviert haben.